Materials International
Open Access Journal (ISSN: 2668-5728)

Review
Volume 7, Issue 1 2025, 10
https://doi.org/10.33263/Materials71.010

Electrochemical Characterizations of Electrode Materials for Supercapacitors

Yogendra Kumar [1,2], Shubham Sharma [1,*], VSR Rajasekhar Pullabhotla [2,*]

[1] Department of Chemistry, GLA University, Mathura-281406
[2] Department of Chemistry, Faculty of Science, Agriculture and Engineering, University of Zululand, South Africa
* Correspondence: rajshubh.9557@gmail.com (V.R.P.); pullabhotlav@unizulu.ac.za (V.R.P);

Scopus Author ID 58598233500
Received: 16.05.2024; Accepted: 2.01.2025; Published: 13.02.2025

Abstract: A supercapacitor is a fascinating electrical device with advanced electrochemical properties, including high energy density, quick charge-discharge rates, remarkable cycle stability, and elevated specific capacitance. These characteristics distinguish a supercapacitor from other comparable electronic devices. Significant research and development efforts by scientists over the past few decades have focused on the electrochemical performance of supercapacitors. These initiatives have resulted in the creation of diverse novel electrode materials. This review emphasizes the electrochemical characterization methods for the electrode materials of supercapacitors.

Keywords: electron transfer process; supercapacitors; materials; characterization; energy storage.

1. Introduction

1.1. Motivation.

The demand for alternative energy sources has increased in recent years due to the imperative to reduce harmful environmental effects and rein in the consumption of global energy resources. The supercapacitors (SCs) have sparked a wide variety of research interests [1-2]. The SCs are just one of many atypical electric-power devices that are used in a wide number of fields, such as hybrid autos and electric mass transit vehicles [3] and wearable/portable electronic gadgets [4-5] due to the remarkable electrochemical capabilities of SCs, which include high specific power, superior cycling life, and quick charging–discharging rate [6-9]. There is a single type of capacitor that goes by many different names; they include ultracapacitors, electrochemical capacitors (ECs), gold capacitors, electrical double-layer capacitors (EDLCs) [10], pseudocapacitors, and power coaches [11-12]. Because of the use of an electrolyte, a current collector, and electrodes with a large specific surface area (SSA) [13-14], the capacitance of an SC is increased by a factor of 10,000 compared to that of a conventional capacitor. Thin dielectric separators [15] also increase the capacitance of SCs compared to standard batteries. The SCs store energy through a charge-discharge mechanism at the electrode-electrolyte interface [16], similar to that of traditional capacitors; however, the charge-discharge process in SCs is significantly faster [17]. While ordinary capacitors may store a charge between micro and millifarads, electrolytic SCs can store a charge between 100 and 1000 F while maintaining a low equivalent series resistance (ESR) and specific power [18].

Suppose properly designed and efficient materials are utilized. In that case, SCs can outperform batteries in specific energy density (SED) and power density (Pd) by many orders of magnitude, making them a versatile energy storage choice [18]. Power density indicates how fast a device can deliver energy, whereas energy density indicates how long an energy storage device may be used.

2. Characterization Techniques for Supercapacitors

2.1. Cyclic voltammetry (CV).

One of the most extensively utilized electrochemical characterization techniques is cyclic voltammetry measurement [19-22]. During a triangle cyclic potential scan in cyclic voltammetry, the electric potential at the electrode surface changes linearly with respect to time. The voltammogram, or current-potential waveform, gives important information on the reactivity of the electrolyte and mass transport capabilities [23-24]. The recorded current profile illustrates the kinetics of chemical reactions in the solution and distinct physical phenomena for ionic transfer when the electrode surface potential varies in a potential window [25-28]. Cyclic voltammetry has been widely used in experimental studies to characterize the electrochemical behavior of anodes, cathodes, and electrolytes in various energy storage devices, including lithium-ion batteries [29-32]. The supercapacitors [33,34], flow batteries [35-36], and fuel cells [37-38]. There are two types of electrode systems for the cyclic voltammetry characterization technique, including three and two electrode systems, respectively, as shown in Figure 1.

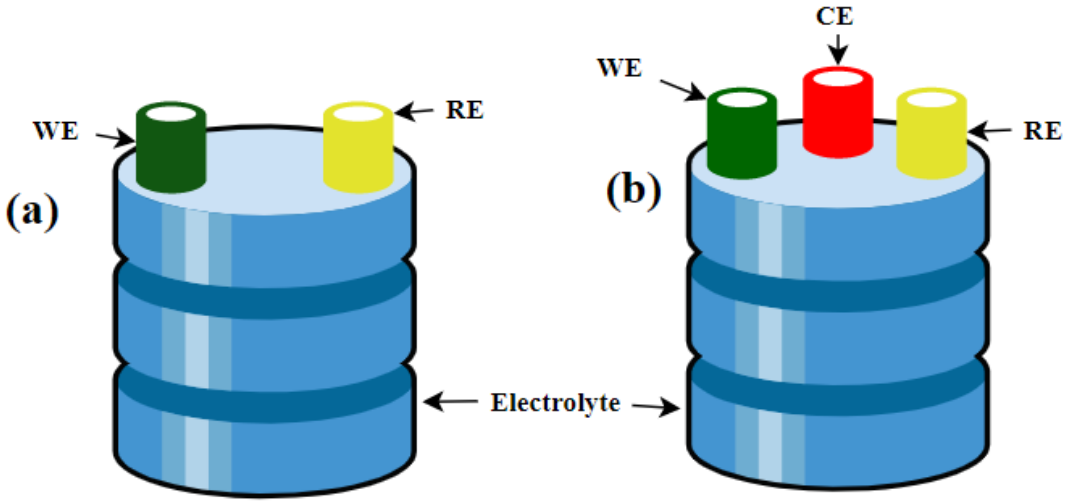

Figure 1. Electrode systems used for potentiometric and volt amperometric measurements **(a)** two electrode system; **(b)** three-electrode system (WE (Working electrode), RE (Reference electrode) and CE (Counter electrode) stands for Working, Reference and Counter Electrodes, respectively) ().

In a three-electrode system (Figure 1b), cyclic voltammetry (CV) is the linearly varying electric potential between reference and working electrodes or between positive and negative electrodes in a two-electrode system, as shown in Figure 1a [39]. The scan rate refers to the pace at which the potential changes, whereas the potential working range is referred to as the potential window [23]. The electrochemical processes and charge storage mechanism are outlined by the current patterns observed during the cathodic/anodic sweeps. In the case of EDLC (electric double-layer capacitor), a rectangular pattern is formed (Figure 2a), whereas significant redox peaks develop in a reversible way in pseudocapacitance materials [40-42], as

illustrated in Figure 2b. The scan rate is related to the instantaneous current generated by the EDL (electric double layer) mechanism. In a three-electrode setup, CV measurements may be used to determine the specific capacitance, the potential window of electrode materials, and the charge/discharge reversibility [43]. Equation 1 can be used to calculate the specific capacitance (C) of a supercapacitor device assessed using the CV technique.

$$C_s = \frac{\int idV}{2km\Delta V} \quad (1)$$

Where C_s is the specific capacitance (F/g), k is the scan rate (mV/S), m is the mass of active electrode material (g), and $\Delta V$is the potential window (V) and $\int idV$ is the area under the CV curve.

A voltammogram is a plot of current against voltage that is usually rectangular for an ideal supercapacitor [44-45], as shown in Figure 2a. The rectangular shape of voltammograms indicates the establishment of an electric double layer, and the overall current density is mostly attributable to capacitive current density. Voltammograms in pseudocapacitors are often quasi-rectangular (Figure 2b), with or without redox peaks. The overall current density of pseudocapacitors is comprised of capacitive and faradaic redox current densities [46]. In real situations, deviations from rectangularity are caused by system series resistance, which can be linked to the electron transfer process in the electrode material, ion diffusion in the electrolyte, and contacts between the electrode and device terminals [47]. Since these resistances prevent the current from responding instantly to changes in the voltage scan directions, two of the voltammogram corners are rounded off to produce a quasi-rectangular shape, as shown in Figures 2b-c, with the rounding becoming more evident as the scan rate is raised. Electrolyte degradation, which usually occurs at the extremes of the voltage scan, is another nonideality typically seen in supercapacitors, as shown in Figure 2c.

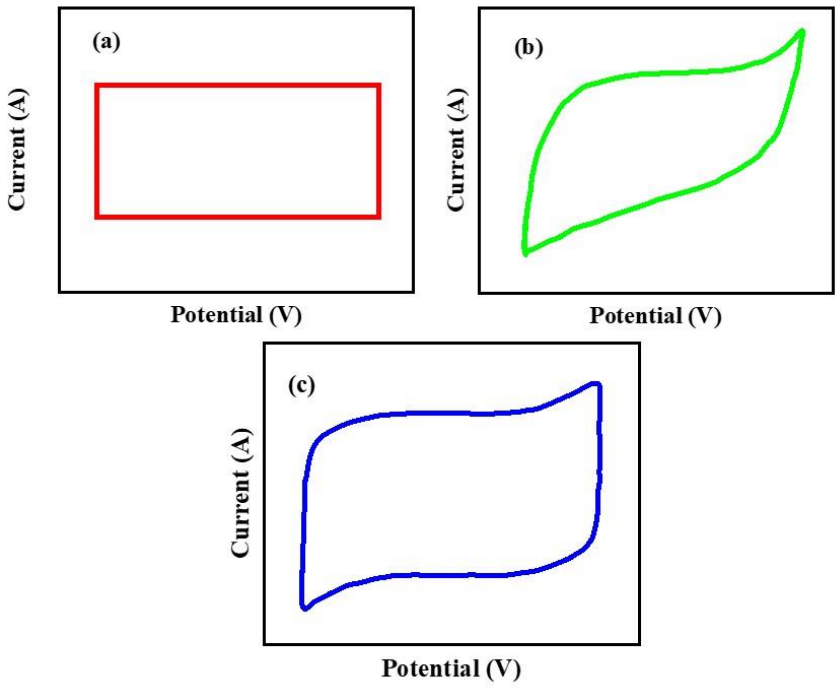

Figure 2. Different types of voltammograms for supercapacitors: **(a)** ideal supercapacitor; **(b)** pseudocapacitors (series resistance); **(c)** non-ideal supercapacitor (electrolyte degradation).

Galvanostatic charge-discharge (GCD) is the experimental *opposite* of cyclic voltammetry, in which the supercapacitor is charged and discharged at a constant applied current between two predetermined voltage points or windows [48]. The GCD characterization

procedure more closely resembles real-world results as it is time-dependent. As shown in Figure 3a, the resultant plot of voltage over time should be linear, with alternating positive and negative slopes. The deviations from linearity can arise for the same reasons as before (for cyclic voltammetry), with series resistance causing the cell voltage (IR drop) to decrease fast when switching from charging to discharging, as shown in Figure 3b. Furthermore, electrolyte deterioration or other redox events, such as pseudocapacitance [49], will result in voltage plot plateaus or inflection points, as indicated in Figure 3c. Moreover, all genuine supercapacitors exhibit self-discharge, which occurs when the device is charged but not linked to any external load and conducts a small amount of current. The parasitic current may be large if the cell is short-circuited via unintended direct contact with the electrodes [50]. Due to the increased relative magnitude of the parasitic current, the cell voltage drops quicker than predicted during discharge. This is especially visible at low applied current densities [51]. The specific capacitance of a supercapacitor for a two-electrode system can be computed using Equation 2:

$$C_s = \frac{2I\Delta t}{m\Delta V} \qquad (2)$$

Where C_s represents the specific gravimetric capacitance (F/g), I represents the discharging current (A), Δt represents the charging/discharging time (s), m represents the mass of the active material (g), and ΔV represents the operating potential window.

GCD testing provides the following performance evaluations for various structures when used in supercapacitor applications: alginate interconnected porous carbon [52-54] had a stable capacitance value with an increase in current density, an increase in pseudo redox processes for porous carbon material obtained from pectin biopolymer [55-56], and high cycle stability for multi-hierarchical porous carbon obtained from keratin biopolymer [57-58]. Galvanostatic cycling, like cyclic voltammetry, may be used to test rate capability across a wide range of current densities. Since supercapacitors are energy storage devices, the charge stored or discharged and energy are essential information often derived from the GCD data. As always expected, the energy-related findings reflect those for capacitance since energy is simply related to capacitance and the voltage at which the charge is added/removed from the system [59]. While significant IR drops (Figure 3b) may cause deviations between capacitance and energy even with appreciable IR drops in metal oxide systems at high currents [60], all the trends and conclusions drawn for capacitance apply equally well for the energy.

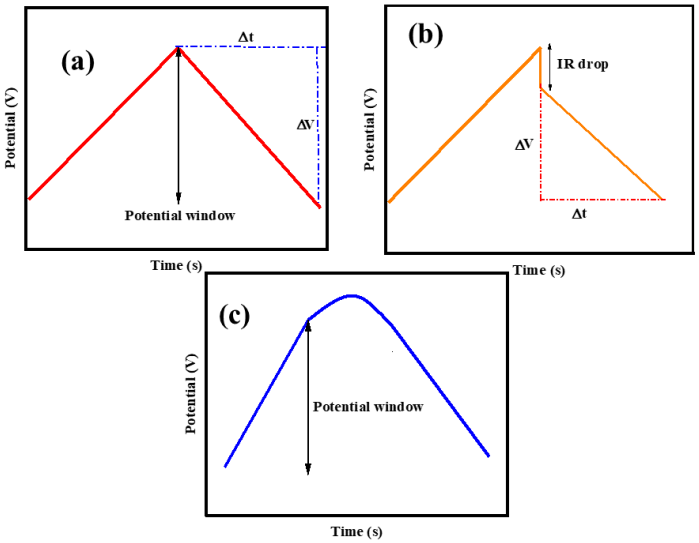

Figure 3. GCD curves **(a)** Ideal supercapacitor; **(b)** Supercapacitor in which there is series resistance; **(c)** Supercapacitor system in which there is electrolyte degradation.

2.3. Electrochemical impedance spectroscopy (EIS).

Electrochemical impedance spectroscopy (EIS) has a number of advantages for determining the power delivery capabilities of supercapacitor devices. In a single experiment, EIS can isolate and measure the reaction bulk (Rb), interface layer, charge transfer reaction (Rct), and diffusion process (W) cell resistances [61]. Measuring EIS spectra does not need the disassembly of the supercapacitor cell, which is beneficial in reducing moisture and oxygen contamination of sensitive samples [61]. It is also feasible to do EIS measurements while the cell operates, which is useful for acquiring spectra without disturbing the cell. A supercapacitor is made up of the following components: a cathode, an anode, a separator, current collectors, and an electrolyte. Electrons and ions travel through each component of the cell that possesses resistive and capacitive characteristics during electrochemical processes. In other words, the circuit elements that make up the equivalent circuit model, which connects these components in parallel and/or series, are the supercapacitor components and the double layer on the interface [62]. Although the impedance characteristics of circuit parts differ depending on cell type and component character[61], the overall impedance value may normally be determined by scanning the AC frequency in the 100 kHz to 10 MHz range [61,63]. The frequency range of EIS analysis is determined by the normal reaction time with the components of the confined cell [64]. As a result, the low frequency of 10 Hz to 10 MHz is used to depict the slow transport process of ion diffusion, which is indicated as Warburg impedance [65], shown in Figure 4b. The impedance associated with the charge transfer reaction may be acquired in the middle-frequency range of 10 kHz to 10 Hz, followed by the normal time's constants, and the relatively quick transport process across the interface layer can be measured in the high-frequency range of 100 kHz to 10 kHz. EIS spectral fitting based on the obtained equivalent circuit model [66] may be used to assess the associated impedance values for each frequency range. The impedance is derived from these measurements at each frequency and displayed as a Nyquist plot (Figure 4a), which graphs the imaginary component of impedance against the real component, or a Bode plot (Figure 4b), which shows the magnitude of impedance and phase shift versus frequency [59,62]. EIS data may be interpreted using multiple supercapacitor equivalent circuit models (Figure 4c). Specific characteristics like EDLC, series resistance (Rs), and charge transfer resistance are associated with redox processes at the electrode/electrolyte interface, assuming pseudocapacitance is relevant and diffusion-related resistance can be derived from the best fit [67].

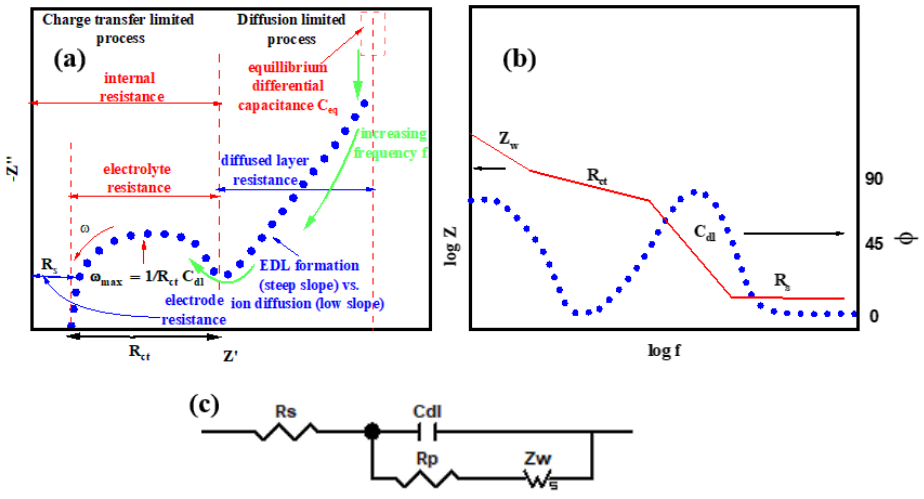

Figure 4. EIS plots **(a)** Nyquist plot; **(b)** Bode plot; **(c)** Equivalent electrical circuit diagram for fitting.

The ideal Randles electrical equivalent circuit of the interface is shown in Figure 4c. On the left in Figure 4a are the high-frequency components, while on the right are the low-frequency components. In Figure 4c, Cdl stands for double-layer capacitor; Rp stands for polarisation resistance; Rs stands for solution resistance; ZW stands for Warburg impedance. The mass transports of the reactant and product have a role in influencing the rate of electron transfer at the interface, which is determined by the consumption of oxidants and the creation of the reductant near the electrode surface. Another sort of impedance (ZW) is provided by the mass transfer of the reactants and products, which may be utilized in CV because it appears as a peak current in a voltammogram. Each circuit component corresponds to each interfacial component, as shown in Figure 4c.

2.4. Specific surface area/porosity and morphology.

The synthesis method utilized for processing biopolymer materials to obtain carbon significantly affects the morphology and surface area of the carbon produced [68-72]. All the synthesis methods aid in achieving a porous carbon but with different qualities (surface area and morphology). Therefore, we will look at the morphological and surface area characterization based on the synthesis techniques. The following characterization techniques are used to assess the morphology and surface area of the active materials: Scanning Electron Microscopy (SEM), Transmission Electron Microscopy (TEM), and Brunauer-Emmett-Teller (BET) technique. To start with, a chemical activation method was used to extract carbon from lignin biopolymer, according to Singh *et al*. [73]. The SEM results of the CA-CNF sample showed a chopped ribbon-like morphology with a short length. A continuous ribbons-like morphology, which split into short-length discontinuous stripes, was obtained for the CNF mats sample as a result of crushing with activating chemicals. CA-CNF, on the other hand, retains its prior ribbon morphology following grinding and activation. The ACNF 2-D mats had a continuous and linked fiber network with a diameter in the nano to sub-micron range (600-1400 nm). The electrochemical behavior of the electrode is influenced by its surface area and porosity type. The specific surface area of the ACNF mat was 806.9 m^2/g, whereas the AC [73] and CA-CNF samples were 1856.8 m^2/g and 1843.9 m^2/g, respectively. Microwave-assisted synthesis was used by Li *et al*. [74] to synthesize carbon from chitosan biopolymer for electrochemical applications. The best NHPC-produced sample has a high nitrogen concentration of 9.4 wt%, a large specific surface area of 1170 m^2/g, a pore volume of 1.32 cm^3/g, and a mesopore ratio of 78%. The pore size of NHPC-2.5 reaches several micrometers, which is significantly larger than that of NHPC-2.0. The microstructure of mesopores and micropores has been established in the NHPC-2.0 sample. As a result, the SEM and TEM images show that NHPC-2.0 has a hierarchically porous structure with macropores, mesopores, and micropores. In addition, thermal treatment was employed to extract carbon from cellulose biopolymer for use in electrochemical energy storage devices by Wang *et al*. [75]. The t-plot technique was used to calculate the specific surface area of micropores, which reached a maximum of 687 m^2/g for HPC-1000 and dropped as the thermal treatment temperature increased. After heat treatment, the Field emission scanning electron microscopy (FESEM) images show a shrunken micro-sized spherical morphology, and the high-magnification FESEM confirms the existence of mesopores in the shrunken microspheres. In another study by Li *et al*. [76] on electrochemical applications of natural biopolymer carbon generated utilizing the template approach, the as-obtained NPCA sample has a honeycomb-like 3D (three-dimensional) network architecture made up of linked carbon nano-sheets with a

hierarchical porous structure and large specific surface area of up to 1438 cm^3/g was achieved. Moreover, Zhou *et al*. [77] also investigated the use of a novel in-situ template approach to produce carbon from pectin biopolymer for energy storage. The NHPC-700 had a large specific surface area of 2928 m^2/g and a good micropore/mesopores ratio, which helped to improve specific capacitance performance. SEM was used to examine the morphology of the as-prepared carbon. The NHPC-600 has an uneven framework structure with numerous interconnecting macropores after being activated at 600°C. When the activation temperature is raised to 700°C or 800°C, the NHPC-700 and NHPC-800 displayed a 3D architecture made up of unevenly ordered thin sheets morphology. The evidence presented thus far supports the idea that the synthesis methods significantly affect the morphology and surface area of the carbon material generated. The walls of the pore in carbon materials appear thin, and the interconnected pores create a networked morphology [76-77]. The activation agent used, which may operate synergistically as a *surfactant* that forms the network while releasing gas upon degradation enables pore connectivity, can be attributed to such distinct structural properties [78]. Closed pores are also detected in carbon synthesized with salt as an activator, probably because no gaseous by-products are produced during carbonization despite the thin walls of the pore [79]. Because charge transfer requires an interconnected porous network, it is desired that carbon with a large surface area and porous morphology is the best candidate for use as an electrode material in supercapacitors [80]. Potential electrode material must contain a large number of three-dimensional, crosslinked pores, especially when compared to carbon, with almost no pores or a closed porous structure [76-77].

3. Conclusions

When the battery cannot deliver energy instantaneously, the supercapacitors can fulfill this role, after which the battery can assume responsibility when a steady energy supply is necessary. This hybrid system will be highly sought after since it can be employed in several innovative energy-related applications in the future. Further research is necessary to advance hybrid electric vehicle systems utilizing hybrid capacitors that integrate the functionalities of batteries and supercapacitors. The hybrid-electric car sector is presently at capacity, although a breakthrough in this domain could enable it to surpass these limitations. Notwithstanding the extensive study conducted in the field, the advancement of high-performance supercapacitors remains nascent. Further research is necessary for supercapacitors to achieve their maximum potential. This study should concentrate on the physics of energy storage and the optimal design of the electrodes. Due to the limited study on this aspect of supercapacitors, we concentrated our review on delivering a comprehensive overview of several electrode materials, assessing their performance in supercapacitors, and delineating the advantages and disadvantages of each. This study illustrates that supercapacitors are rapidly emerging as competitive energy storage for future purpose technology owing to significant recent developments in electrode materials. These developments have markedly enhanced supercapacitor performance, enabling them to store considerably greater amounts of energy in the future.

Funding

This research received no external funding.

Acknowledgments

The authors are very thankful to GLA University, Mathura, for providing infrastructural and financial support. The technical support rendered by Dr. Anuj Kumar is gratefully acknowledged.

Conflicts of Interest

The authors declare no conflict of interest.

References

1. Rani, N.; Yadav, S.; Mushtaq, A.; Rani, S.; Saini, M.; Rawat, S.; Maity, D. Azadirachta indica peel extract-mediated synthesis of ZnO nanoparticles for antimicrobial, supercapacitor and photocatalytic applications. *Chem. Pap.* **2024**, *78*, 3687-3704, https://doi.org/10.1007/s11696-024-03340-6.
2. Kumar, Y. A., Roy, N., Ramachandran, T., Hussien, M., Moniruzzaman, M., & Joo, S. W. Shaping the future of energy: The rise of supercapacitors progress in the last five years. *Journal of Energy Storage*, **2024**, *98*, 113040, https://doi.org/10.1016/j.est.2024.113040
3. Burke, A.; Liu, Z.; Zhao, H. Present and future applications of supercapacitors in electric and hybrid vehicles. In Proceedings of the 2014 IEEE International Electric Vehicle Conference (IEVC), 17-19 Dec. 2014, **2014**; pp. 1-8, https://doi.org/10.1109/IEVC.2014.7056094.
4. Sharma, P.; Kumar, V. Current technology of supercapacitors: A review. *J. Electron. Mater*. **2020**, *49*, 3520-3532, https://doi.org/10.1007/s11664-020-07992-4.
5. Vashistha, V. K.; Bala, R.; Mittal, A.; Das, D. K.; Sharma, S.; Pullabhotla, R. V. Nanocomposite based Electrochemical Sensors for Determination of Some Biologically Important Compounds: A Review. *Anal. Bioanal. Chem.* **2023**, *15*, 668-695, https://doi.org/10.22034/abec.2023.707326.
6. Kim, B.K.; Sy, S.; Yu, A.; Zhang, J. Electrochemical Supercapacitors for Energy Storage and Conversion. In Handbook of Clean Energy Systems; **2015**; pp. 1-25, https://doi.org/10.1002/9781118991978.hces112.
7. Yadlapalli, R. T., Alla, R. R., Kandipati, R., & Kotapati, A. Super capacitors for energy storage: Progress, applications and challenges. *Journal of Energy Storage*, **2022**, *49*, 104194, https://doi.org/10.1016/j.est.2022.104194
8. Dhas, S. D., Thonge, P. N., Mendhe, A. C., Yun, J., & Kim, D. Nickel manganite-based materials for electrochemical supercapacitors: An overview. *Renewable and Sustainable Energy Reviews*, **2024**, *204*, 114819, https://doi.org/10.1016/j.rser.2024.114819
9. Molahalli, V., Chaithrashree, K., Singh, M. K., Agrawal, M., Krishnan, S. G., & Hegde, G. Past decade of supercapacitor research–lessons learned for future innovations. *Journal of Energy Storage*, **2023**, *70*, 108062, https://doi.org/10.1016/j.est.2023.108062.
10. Schutter, C.; Pohlmann, S.; Balducci, A. Industrial requirements of materials for electrical double layer capacitors: impact on current and future applications. *Adv. Energy Mater.* **2019**, *9*, 1900334, https://doi.org/10.1002/aenm.201900334.
11. Yaseen, M.; Khattak, M.A.K.; Humayun, M.; Usman, M.; Shah, S.S.; Bibi, S.; Hasnain, B.S.U.; Ahmad, S.M.; Khan, A.; Shah, N.; Tahir, A.A. A review of supercapacitors: materials design, modification, and applications. *Energies* **2021**, *14*, 7779, https://doi.org/10.3390/en14227779.
12. Emilia, G.; Krzysztof, W. Recent Progress on Electrochemical Capacitors Based on Carbon Nanotubes. In Carbon Nanotubes, Mohammed Muzibur, R., Abdullah Mohamed, A., Eds.; IntechOpen: Rijeka, **2017**; p. Ch. 9, https://doi.org/10.5772/intechopen.71687.
13. Zheng, C.; Zhou, X.; Cao, H.; Wang, G.; Liu, Z. Synthesis of porous graphene/activated carbon composite with high packing density and large specific surface area for supercapacitor electrode material. *J. Power Sources* **2014**, *258*, 290-296, https://doi.org/10.1016/j.jpowsour.2014.01.056.
14. Niu, J.; Shao, R.; Liang, J.; Dou, M.; Li, Z.; Huang, Y.; Wang, F. Biomass-derived mesopore-dominant porous carbons with large specific surface area and high defect density as high performance electrode materials for Li-ion batteries and supercapacitors. *Nano energy* **2017**, *36*, 322-330, https://doi.org/10.1016/j.nanoen.2017.04.042.
15. Carlson, T.; Asp, L.E. Structural carbon fibre composite/PET capacitors-Effects of dielectric separator thickness. *Composites, Part B.* **2013**, *49*, 16-21, https://doi.org/10.1016/j.compositesb.2013.01.009.

16. Leng, C.; Zhao, Z.; Song, Y.; Sun, L.; Fan, Z.; Yang, Y.; Liu, X.; Wang, X.; Qiu, J. 3D carbon frameworks for ultrafast charge/discharge rate supercapacitors with high energy-power density. *Nano-micro letters*. **2021**, *13*, 1-11, http://dx.doi.org/10.1007/s40820-020-00535-w.
17. Wang, R.; Lang, J.; Zhang, P.; Lin, Z.; Yan, X. Fast and large lithium storage in 3D porous VN nanowires-Graphene composite as a superior anode toward high-performance hybrid Supercapacitors. *Adv. Funct. Mater*. **2015**, *25*, 2270-2278, https://doi.org/10.1002/adfm.201404472.
18. Yang, H.; Kannappan, S.; Pandian, A.S.; Jang, J.H.; Lee, Y.S.; Lu, W. Graphene supercapacitor with both high power and energy density. *Nanotechnology* **2017**, *28*, 445401, https://doi.org/10.1088/1361-6528/aa8948.
19. Joshi, P.S.; Sutrave, D. S. Building an Arduino based potentiostat and Instrumentation for Cyclic Voltammetry. *J. Appl. Sci. Comput* **2018**, *5*, 163-167.
20. dos Santos, J. P. A., Rufino, F. C., Ota, J. I. Y., Fernandes, R. C., Vicentini, R., Pagan, C. J., ... & Zanin, H. Best practices for electrochemical characterization of supercapacitors. *Journal of Energy Chemistry*, **2023**, *80*, 265-283. https://doi.org/10.1016/j.jechem.2022.12.034
21. Rafiee, M., Abrams, D. J., Cardinale, L., Goss, Z., Romero-Arenas, A., & Stahl, S. S. Cyclic voltammetry and chronoamperometry: mechanistic tools for organic electrosynthesis. *Chemical Society Reviews*, **2024**, https://doi.org/10.1039/D2CS00706A.
22. Periasamy, V., Elumalai, P. N. N., Talebi, S., Subramaniam, R. T., Kasi, R., & Iwamoto, M. Novel same-metal three electrode system for cyclic voltammetry studies. *RSC advances*, **2023**, *13*(9), 5744-5752; 10.1039/D3RA00457K
23. Aderyani, S.; Flouda, P.; Shah, S.A.; Green, M.J.; Lutkenhaus, J. L.; Ardebili, H.; Simulation of cyclic voltammetry in structural supercapacitors with pseudocapacitance behavior. *Electrochim. Acta* **2021**, *390*, 138822, https://doi.org/10.1016/j.electacta.2021.138822.
24. Sarabia, F. J.; Sebastián-Pascual, P.; Koper, M.T.; Climent V.; Feliu, J.M. Effect of the interfacial water structure on the hydrogen evolution reaction on Pt(III) modified with different nickel hydroxide coverages in alkaline media. *ACS Appl. Mater. Interfaces* **2018**, *11*, 613-623, https://doi.org/10.1021/acsami.8b15003.
25. Bao, D.; Zhang, Q.; Meng, F.L.; Zhong, H.X.; Shi, M.M.; Zhang, Y.; Yan, J.M.; Jiang, Q.; Zhang, X.B. Electrochemical reduction of N_2 under ambient conditions for artificial N_2 fixation and renewable energy storage using N_2/NH_3 cycle. *Adv. Mater*. **2017**, *29*, 1604799, https://doi.org/10.1002/adma.201604799.
26. Bhuvanendran, N., Ravichandran, S., Xu, Q., Maiyalagan, T., & Su, H. A quick guide to the assessment of key electrochemical performance indicators for the oxygen reduction reaction: A comprehensive review. *International Journal of Hydrogen Energy*, 2022, *47*(11), 7113-7138, https://doi.org/10.1016/j.ijhydene.2021.12.072
27. Jaugstetter, M., Blanc, N., Kratz, M., & Tschulik, K. Electrochemistry under confinement. *Chemical Society Reviews*, **2022**, *51*(7), 2491-2543, 10.1039/D1CS00789K
28. Pholauyphon, W., Charoen-amornkitt, P., Suzuki, T., & Tsushima, S. Guidelines for supercapacitor electrochemical analysis: A comprehensive review of methodologies for finding charge storage mechanisms. *Journal of Energy Storage*, **2024**, *98*, 112833, https://doi.org/10.1016/j.est.2024.112833.
29. Chen, L.F.; Lu, Y.; Yu, L.; Lou, X.W.D. Designed formation of hollow particle-based nitrogen-doped carbon nanofibers for high-performance supercapacitors. *Energy Environ. Sci.* **2017**, *10*, 1777-1783, https://doi.org/10.1039/C7EE00488E.
30. Tie, D.; Huang, S.; Wang, J.; Ma, J.; Zhang, J.; Zhao, Y. Hybrid energy storage devices: Advanced electrode materials and matching principles. *Energy Storage Mater*. **2019**, *21*, 22-40, https://doi.org/10.1016/j.ensm.2018.12.018.
31. Chen, W.; Li, G.; PeiLi, A.Y.; Liao, L.; Wang, H.; Wan, J.; Liang, Z.; Chen, G.; Zhang, H.; Wang, J. A manganese-hydrogen battery with potential for grid-scale energy storage. *Nat. Energy* **2018**, *3*, 428-435, https://doi.org/10.1038/s41560-018-0147-7.
32. Palchoudhury, S.; Ramasamy, K.; Gupta, R.K.; Gupta, A. Flexible supercapacitors: a materials perspective. *Front. Mater*. **2019**, *5*, 83, https://doi.org/10.3389/fmats.2018.00083.
33. Giannakou, P.; Slade, R.C.; Shkunov, M. Cyclic Voltammetry Studies of Inkjet- printed NiO supercapacitors: Effect of substrates, printing and materials. *Electrochim. Acta*. **2020**, *353*, 136539, https://doi.org/10.1016/j.electacta.2020.136539.
34. Kumar, S.; Dhaliwal, A.S. Cyclic Voltammetry Synthesis of Polyaniline as Supercapacitors Electrode. *Materials Today: Proceedings* **2020**, *21*,1833-1839, https://doi.org/10.1016/j.matpr.2020.01.238.
35. Loupe, N.; Doan, J.; Gurau, B.; Smotkin, E.S. Electrochemical Energy Storage: Current and Emerging Technologies. In Handbook of Industrial Chemistry and Biotechnology, Kent, J.A., Bommaraju, T.V.,

Barnicki, S.D., Eds.; Springer International Publishing: Cham, **2017**; pp. 1695-1727, https://doi.org/10.1007/978-3-319-52287-6_31.

36. Zhang, L., Feng, R., Wang, W., & Yu, G. Emerging chemistries and molecular designs for flow batteries. *Nature Reviews Chemistry*, **2022**, *6*(8), 524-543, https://doi.org/10.1038/s41570-022-00394-6
37. Gudavalli, G.S.; Dhakal, T.P. Chapter 8 - Simple Parallel-Plate Capacitors to High–Energy Density Future Supercapacitors: A Materials Review. In Emerging Materials for Energy Conversion and Storage, Cheong, K.Y., Impellizzeri, G., Fraga, M.A., Eds.; Elsevier: **2018**; pp. 247-301, https://doi.org/10.1016/B978-0-12-813794-9.00008-9.
38. Qasem, N. A., & Abdulrahman, G. A. A recent comprehensive review of fuel cells: history, types, and applications. *International Journal of Energy Research*, **2024**, *2024*(1), 7271748, https://doi.org/10.1155/2024/7271748
39. Deylaminezhad, M.; Zakipour, M.; Doroodmand, M.M.; Mehrtash, M. Selective storage and evolution of hydrogen on nafion/NaCl/graphene quantum dot mixed matrix using tensammetry as power electrochemical technique. *Int. J. Hydrogen Energy* **2017**, *42*, 9428-9439, https://doi.org/10.1016/j.ijhydene.2017.02.067.
40. Van Lam, D.; Sohail, M.; Kim, J.H.; Lee, H.J.; Han, S.O.; Shin, J.; Kim, D.; Kim, H.; Lee, S.M. Laser synthesis of MOF-derived Ni@ Carbon for high-performance pseudocapacitors. *ACS Appl. Mater. Interfaces* **2020**, *12*, 39154-39162, https://doi.org/10.1021/acsami.0c10235.
41. Liu, Y.; Jiang, S.P.; Shao, Z. Intercalation pseudocapacitance in electrochemical energy storage: recent advances in fundamental understanding and materials development. *Mater. Today Adv.* **2020**, *7*, 100072, https://doi.org/10.1016/j.mtadv.2020.100072.
42. Kumar, S.; Saeed, G.; Zhu, L.; Hui, K.N.; Kim, N.H.; Lee, J.H. 0D to 3D carbon-based networks combined with pseudocapacitive electrode material for high energy density supercapacitor: A review. *Chem. Eng. Jour*. **2021**, *403*, 126352, https://doi.org/10.1016/j.cej.2020.126352.
43. Stoller, M.D.; Ruoff, R.S. Best practice methods for determining an electrode material's performance for ultracapacitors. *Energy Environ. Sci.* **2010**, *3*, 1294-1301, https://doi.org/10.1039/C0EE00074D.
44. Guo, T., Zhou, D., Pang, L., Sun, S., Zhou, T., & Su, J, Perspectives on working voltage of aqueous supercapacitors. *Small*, **2022**, *18*(16), 2106360, https://doi.org/10.1002/smll.202106360.
45. Iqbal, M. Z., & Aziz, U, Supercapattery: Merging of battery-supercapacitor electrodes for hybrid energy storage devices. *Journal of Energy Storage*, **2022**, *46*, 103823, https://doi.org/10.1016/j.est.2021.103823 .
46. Oje, A.M.; Ogwu, A.A.; Rahman, S.U.; Oje, A.I.; Tsendzughul, N. Effect of temperature variation on the corrosion behaviour and semiconducting properties of the passive film formed on chromium oxide coatings exposed to saline solution. *Corros. Sci.* **2019**, *154*, 28-35, https://doi.org/10.1016/j.corsci.2019.04.004.
47. Xu, Z.; Sun, S.; Cui, W.; Lv, J.; Geng, Y.; Li, H.; Deng, J. Interconnected network of ultrafine MnO2 nanowires on carbon cloth with weed-like morphology for high- performance supercapacitor electrodes. *Electrochim. Acta* **2018**, *268*, 340-346, https://doi.org/10.1016/j.electacta.2018.02.138.
48. Bahuguna, G.; Ram, P.; Sharma, R.K.; Gupta, R. An organo-fluorine compound mixed electrolyte for ultrafast electric double layer supercapacitors. *ChemElectroChem* **2018**, *5*, 2767-2773, https://doi.org/10.1002/celc.201800908.
49. Sunil, V.; Jose, R. Hybrid Nanocomposite Metal Oxide Materials for Supercapacitor Application. In Chemically Deposited Nanocrystalline Metal Oxide Thin Films: Synthesis, Characterizations, and Applications, Ezema, F.I., Lokhande, C.D., Jose, R., Eds.; Springer International Publishing: Cham, **2021**; pp. 673-724, https://doi.org/10.1007/978-3-030-68462-4_25.
50. Pandey, G.P.; Klankowski, S.A.; Liu, T.; Wu, J.; Li, J. Toward highly stable solid-state unconventional thin-film battery-supercapacitor hybrid devices: Interfacing vertical core- shell array electrodes with a gel polymer electrolyte. *J. Power Sources* **2017**, *342*, 1006-1016, https://doi.org/10.1016/j.jpowsour.2017.01.022.
51. Lee, H.; Kumbhar, V.S.; Lee, J.; Choi, Y.; Lee, K. Highly reversible crystal transformation of anodized porous V_2O_5 nanostructures for wide potential window high-performance supercapacitors. *Electrochim. Acta* **2020**, *334*, 135618, https://doi.org/10.1016/j.electacta.2020.135618.
52. Sun, S.; Han, F.; Wu, X.; Fan, Z. One-step synthesis of biomass derived O, N-codoped hierarchical porous carbon with high surface area for supercapacitors. *Chin. Chem. Lett.* **2020**, *31*, 2235-2238, https://doi.org/10.1016/j.cclet.2019.11.023.
53. Wei, K.; Zhang, F.; Yang, Y.; Zhai, B.; Wang, X.; Song, Y. Oxygenated N-doped porous carbon derived from ammonium alginate: Facile synthesis and superior electrochemical performance for supercapacitor. *J. Energy Storage* **2022**, *51*, 104342, https://doi.org/10.1016/j.est.2022.104342.

54. Xia, L.; Huang, H.; Fan, Z.; Hu, D.; Zhang, D.; Khan, A.S.; Usman, M.; Pan, L. Hierarchical macro-/meso-/microporous oxygen-doped carbon derived from sodium alginate: A cost-effective biomass material for binder-free supercapacitors. *Mater. Des* **2019**, *182*, 108048, https://doi.org/10.1016/j.matdes.2019.108048.
55. Bakhtiarian, M.; Khodaei M.M. Sonochemical synthesis of 1, 4-dihydropyridines using a bio-derived magnetic nanocomposite based on the pectin modified with the di-sulfonic acids under mild conditions. *Mater. Today Commun*. **2021**, *29*, 102791, https://doi.org/10.1016/j.mtcomm.2021.102791.
56. Xu, L.; Cui, L.; Jia, M.; Li, Y.; Gao, J.; Jin, X. Self-assembly of flexible grapheme hydrogel electrode based on crosslinked pectin-cations. *Carbohydr. Polym.* **2018**, *195*, 593-600, https://doi.org/10.1016/j.carbpol.2018.04.078.
57. Sinha, P.; Yadav, A.; Tyagi, A.; Paik, P.; Yokoi, H.; Naskar, A.K.; Kuila, T.; Kar, K.K. Keratin-derived functional carbon with superior charge storage and transport for high-performance supercapacitors. *Carbon* **2020**, *168*, 419-438, https://doi.org/10.1016/j.carbon.2020.07.007.
58. Wu, S.; Zhou, H.; Zhou, Y.; Wang, H.; Li, Y.; Liu, X.; Zhou, Y. Keratin-derived heteroatoms-doped hierarchical porous carbon materials for all-solid flexible supercapacitors. *J. Alloys Compd.* **2021**, *859*, 157814, https://doi.org/10.1016/j.jallcom.2020.157814.
59. Han, X.; Liao, F.; Zhang, Y.; Han, X.; Xu, C.; Chen, H. Solvothermal preparation of zinc cobaltite mesoporous microspheres for high-performance electrochemical supercapacitors. *J. Alloys Compd* **2019**, *781*, 425, https://doi.org/10.1016/j.jallcom.2018.12.079.
60. Dujearic-Stephane, K.; Gupta, M.; Kumar, A.; Sharma, V.; Pandit, S.; Bocchetta, P.; Y. Kumar. The effect of modifications of activated carbon materials on the capacitive performance: surface, microstructure, and wettability. *J. Compos. Sci.* **2021**, *5*, 66, https://doi.org/10.3390/jcs5030066.
61. Choi, W.; Shin, H.C.; Kim, J.M.; Choi, J.Y.; Yoon, W.S. Modeling and applications of electrochemical impedance spectroscopy (EIS) for lithium-ion batteries. *J. Electrochem. Sci. Technol*. **2020**, *11*, 1-13.
62. Mainka, J.; Gao, W.; He, N.; Dillet, J.; Lottin, O. A General Equivalent Electrical Circuit Model for the characterization of MXene/graphene oxide hybrid-fiber supercapacitors by electrochemical impedance spectroscopy–Impact of fiber length. *Electrochim. Acta* **2022**, *404*, 139740, https://doi.org/10.1016/j.electacta.2021.139740.
63. Navalpotro, P.; Anderson, M.; Marcilla, R.; Palma, J. Insights into the energy storage mechanism of hybrid supercapacitors with redox electrolytes by Electrochemical Impedance Spectroscopy. *Electrochim. Acta* **2018**, *263*, 110, https://doi.org/10.1016/j.electacta.2017.12.167.
64. Barai, A.; Uddin, K.; Widanage, W.D.; McGordon, A.; Jennings, P. A study of the influence of measurement timescale on internal resistance characterisation methodologies for lithium-ion cells. *Sci. Rep.* **2018**, *8*, 21, https://doi.org/10.1038/s41598-017-18424-5.
65. Samukaite-Bubniene, U.; Valiūniene, A.; Bucinskas, V.; Genys, P.; Ratautaite, V.; Ramanaviciene, A.; Aksun, E.; Tereshchenko, A.; Zeybek, B.; Ramanavicius, A. Towards supercapacitors: Cyclic voltammetry and fast Fourier transform electrochemical impedance spectroscopy-based evaluation of polypyrrole electrochemically deposited on the pencil graphite electrode. *Colloids Surf., A* **2021**, *610*, 125750, https://doi.org/10.1016/j.colsurfa.2020.125750.
66. Krewer, U.; Roder, F.; Harinath, E.; Braatz, R.D.; Bedurftig, B.; Findeisen, R. Dynamic models of Li-ion batteries for diagnosis and operation: a review and perspective. *J. Electrochem. Soc.* **2018**, *165*, A3656, https://doi.org/10.1149/2.1061814jes.
67. Majumder, M.; Choudhary, R.B.; Thakur, A.K.; Khodayari, A.; Amiri, M.; Boukherroub R.; Szunerits, S. Aluminum based metal-organic framework integrated with reduced graphene oxide for improved supercapacitive performance. *Electrochim. Acta* **2020**, *353*, 136609, https://doi.org/10.1016/j.electacta.2020.136609.
68. Xia, M.; Chen, W.; Wu, J.; Chen, Y.; Yang, H.; Chen, X.; Zhu, D.; Chen, H. Organic salt-assisted pyrolysis for preparation of porous carbon from cellulose, hemicellulose and lignin: New insight from structure evolution. *Fuel* **2021**, *291*, 120185, https://doi.org/10.1016/j.fuel.2021.120185.
69. Kebabsa, L.; Kim, J.; Lee, D.; Lee, B. Highly porous cobalt oxide-decorated carbon nanofibers fabricated from starch as free-standing electrodes for supercapacitors. *Appl. Surf. Sci.* **2020**, *511*, 145313, https://doi.org/10.1016/j.apsusc.2020.145313.
70. Pandi, K.; Prabhu, S.M.; Ahn, Y.; Park, C.M.; Choi, J. Design and synthesis of biopolymer-derived porous graphitic carbon covered iron-organic frameworks for depollution of arsenic from waters. *Chemosphere* **2020**, *254*, 126769, https://doi.org/10.1016/j.chemosphere.2020.126769.

71. Lin, L.; Chen, J.; Mitra, R.; Gao, Q.; Cheng, F.; Xu, T.; Zuo, Z.; Xiang, H.; Han, J. Optimising PHBV biopolymer production in haloarchaea via CRISPRi-mediated redirection of carbon flux. *Commun. Biol.* **2021**, *4*, 1007, https://doi.org/10.1038/s42003-021-02541-z.
72. Agrawal, R.; Kumar, A.; Singh, S.; Sharma, K. Recent advances and future perspectives of lignin biopolymers. *Jour. Pol. Res.* **2022**, *29*, 222, https://doi.org/10.1007/s10965-022-03068-5.
73. Singh, M.; Gupta, A.; Sundriyal, S.; Dubey, P.; Jain, K.; Dhakate, S.R. Activated green carbon-based 2-D nanofabric mats for ultra-flexible all-solid-state supercapacitor. *J. Energy Storage* **2022**, *49*, 104193, https://doi.org/10.1016/j.est.2022.104193.
74. Li, B.; Cheng, Y.; Dong, L.; Wang, Y.; Chen, J.; Huang, C.; Wei, D.; Feng, Y.; Jia, D.; Zhou, Y. Nitrogen doped and hierarchically porous carbons derived from chitosan hydrogel via rapid microwave carbonization for high-performance supercapacitors. *Carbon* **2017**, *122*, 592-603, https://doi.org/10.1016/j.carbon.2017.07.009.
75. Wang, C.; Wang, X.; Lu, H.; Li, H.; Zhao, X.S. Cellulose-derived hierarchical porous carbon for high-performance flexible supercapacitors. *Carbon* **2018**, *140*, 139-147, https://doi.org/10.1016/j.carbon.2018.08.032.
76. Liu, J.; Liu, Y.; Li, P.; Wang, L.; Zhang, H.; Liu, H.; Liu, J.; Wang, Y.; Tian, W.; Wang, X.; Li, Z. Fe-N-doped porous carbon from petroleum asphalt for highly efficient oxygen reduction reaction. *Carbon* **2018**, *126*, 1-8, https://doi.org/10.1016/j.carbon.2017.10.004.
77. Zhou, Y.; Ren, X.; Du, Y.; Jiang, Y.; Wan, J.; Ma, F. In-situ template cooperated with urea to construct pectin-derived hierarchical porous carbon with optimized pore structure for supercapacitor. *Electrochim. Acta* **2020**, *355*, 136801, https://doi.org/10.1016/j.electacta.2020.136801.
78. Li, S.; Cheng, C.; Zhao, X.; Schmidt, J.; Thomas, A. Active salt/silica-templated 2D mesoporous FeCo-Nx-carbon as bifunctional oxygen electrodes for zinc–air batteries. *Angew. Chem. Int. Ed.* **2018**, *57*, 1856-1862, https://doi.org/10.1002/anie.201710852.
79. Zhong, Y.; Wang, T.; Yan, M.; Huang, X.; Zhou, X. Carbon nanofibers derived from cellulose via molten-salt method as supercapacitor electrode. *Int. J. Biol. Macromol*. **2022**, *207*, 541-548, https://doi.org/10.1016/j.ijbiomac.2022.03.048.
80. Ho, K.C.; Lin, L.Y. A review of electrode materials based on core–shell nanostructures for electrochemical supercapacitors. *J. Mater. Chem. A* **2019**, *7*, 3516-3530, https://doi.org/10.1039/C8TA11599K.